# ESR Microscopy and Nanoscopy with "Induction" Detection

Aharon Blank[a,b,]* and Jack H. Freed[b]

[a]Department of Chemistry, Technion—Israel Institute of Technology, Haifa 32000, Israel
[b]National Biomedical Center for Advanced ESR Technology, Department of Chemistry and Chemical Biology,
Cornell University, Ithaca, New York 14853, USA

**Abstract**. The current state-of-the-art in the fields of Nuclear Magnetic Resonance (NMR) and Electron Spin Resonance (ESR) micro-imaging is reviewed. Special attention is given to the uniqueness and the advantages of the conventional "induction" detection method with respect to other emerging sensitive magnetic resonance detection and imaging techniques. Following this, a theoretical description of the factors affecting the sensitivity and resolution in induction detection ESR is provided. Based on the theory, new approaches to substantially improve ESR capabilities, both at room temperature and at low cryogenic temperatures, are discussed. Representative results of experiments conducted at room temperature and at frequencies of 10–16 GHz show that with test samples, a sensitivity of $\sim 10^7$ electron spins and a resolution of $\sim 3$ microns are currently available. The results confirm the validity of the theoretical approach and confirm the value of striving for even higher frequencies and lower temperatures, in order to further improve the performance Finally, some of the current and potential applications of ESR microscopy and nanoscopy (involving imaging with a resolution of $\sim 100$ nm or better) are presented.

## INTRODUCTION

Most knowledge in the natural sciences has been obtained or derived by careful observations and measurements of natural phenomena. One of the most powerful observation methods, which stands out among the "leaders of the pack," is magnetic resonance (MR). MR, which mainly involves two techniques, Nuclear Magnetic Resonance (NMR) and Electron Spin Resonance (ESR), has applications ranging from chemical structure determination[1,2] to medical imaging[3,4] and quantum computing.[5,6] From a scientific point of view, MR was the main focus of at least seven Nobel prizes in physics,[7–10] chemistry,[11,12] and medicine.[13] From an industrial point of view, MR is a multibillion dollar industry, with a wide range of medical (Magnetic Resonance Imaging, MRI) and chemical applications (NMR and ESR spectrometers).

Despite the fact that magnetic resonance was discovered more than 60 years ago, and MRI is more than 30 years old, there is still "plenty of room at the bottom"[14] for new methodologies, approaches, and applications.

For example, currently MR is known to be a very effective but nevertheless very insensitive spectroscopic tool, which requires relatively large amounts of material (several billion molecules) for spectroscopic evaluation. With conventional NMR, the most sensitive experiments have been able to detect $\sim 10^{12}$ spins,[15] while in ESR one can detect $\sim 10^7$ spins.[16] Furthermore, the spatial resolution in MRI and ESR Imaging (ESRI) is limited to $\sim 0.1$–$0.2$ mm with in-vivo applications (small animals),[3,16,17] and $\sim 5$–$10$ μm with small cells and in materials science applications.[16,18,19] The term "conventional" is related here to "induction" detection methods (i.e., by means of a pick up coil or a microwave resonator) for acquiring the MR signal, as used in all modern MR spectrometers and imaging devices.

In recent years there has been an "explosion" in the field of new sensitive MR detection techniques. Methods based upon Hall probe measurements,[20] magnetic resonance force detection,[21–23] Scanning-Tunneling-

*Author to whom correspondence should be addressed.
E-mail: ab59@tx.technion.ac.il

Microscopy (STM)-ESR,[24,25] and Superconducting Quantum Interference Device (SQUID) detection[26] have all approached or surpassed the sensitivity and resolution obtained by the conventional "induction" detection method. Nevertheless, this sensitivity comes with a price, and each one of the new detection methods bears with it some significant limitations. For example, the sensitivity of Hall probes and SQUIDs degrades substantially as the frequency is elevated, and it also depends strongly on the operating temperature. In addition, to make use of the high sensitivity in imaging applications, these detection methods require sequential "point to point" measurements, which are very inconvenient and limited, especially for 3D imaging. STM-ESR works only under high vacuum and ultra-low temperatures, and requires that the samples be deposited on a conductive surface. It cannot provide 3D images, and it also has to scan the surface point-by-point. The most advanced results in terms of sensitivity and resolution were obtained with magnetic resonance force detection, which recently demonstrated a single electron spin sensitivity and a 1D resolution of ~25 nm.[23] However, impressive as they are, these capabilities are still far from being useful for MR spectroscopy and for most imaging applications, due to the required ultra-low cryogenic temperature (1.4 K), high vacuum, complicated sample preparation procedure, limited 3D imaging capability (resolution and sensitivity degrade fast with increasing distance from the probe), and, most importantly, the loss of spectroscopic information due to the high gradients necessary for the detection process. Recently, there were attempts to overcome the gradient-related spectroscopy problem by employing a novel homogenous static field magnetic resonance force detection scheme.[27] However, these efforts have not yet proved to be successful in terms of the sensitivity and spatial resolution they can provide, which are currently still far inferior to the standard practice of common induction detection-based systems.

It can be concluded that despite the many new ideas and the vast activity in the field, induction detection remains the only general-purpose approach available today for both spectroscopy and imaging applications. In view of this, we concluded that future efforts should concentrate on improving the capability of induction detection to provide enhanced MR sensitivity and resolution, as distinct from developing one of these new and "exotic" techniques. With the above notion in mind, it was decided that the first "line of action" will be to greatly improve the sensitivity and resolution of induction detection in ESR. This paper will present our general approach for improving the sensitivity and the resolution, our recent experimental results, and the prospective for the future. In addition, we will describe in detail several types of applications that motivate this activity.

## ESR MICROSCOPY

Nuclear Magnetic Resonance (NMR) microscopy is a well-established field in materials, biological, and medical science, which employs "scaled-down" techniques of Magnetic Resonance Imaging (MRI) with large gradients in high magnetic fields to enable high image resolution.[28] Commercial NMR microscopes/imaging probes are available from several vendors (e.g., Bruker, Varian, Doty Scientific) and are used for the characterization of polymers and tissues, non-invasive tracing of unicellular organisms, investigation of transport phenomena, histological-like applications and much more, with practical resolution limits of ~[10–20 μm]³. [29–34] Two primary factors limiting the resolution in NMR microscopy are the diminishing signal from a small imaged voxel, and the diffusion of the spin-bearing molecules over the long timescale of NMR (e.g., $T_2$'s ~ ms).[18,33,35]

Whereas the field of NMR microscopy is well developed, ESR microscopy, which also aims at imaging with micron-scale resolution, is not a common practice. ESR has inherently many potential virtues over NMR, which could make this a technique of choice for microscopic applications. For example, the signal per spin is much stronger than in NMR,[36] diffusion does not limit the resolution in the short timescales ($T_2$'s ~ μs) of the ESR measurements,[37–39] ESR micro-resonators detect with a quality factor ($Q$) of ~1000 compared to the $Q$ of ~10 of the NMR micro-coils,[28,40] and the ESR line shape is more sensitive to dynamic effects, leading to richer information.[41,42] An additional factor is the low cost of the electromagnets used in ESR as compared to the expensive superconducting magnets of NMR. Since most samples do not contain stable free radicals, these paramagnetic species must be added in a manner similar to that of adding contrast agents in NMR or dyes in optics. This is a standard procedure, especially for microscopy, which eliminates any concerns with a large undesirable background signal, (such as protons in NMR). These fundamental advantages led us to consider the use of ESR microscopy as an alternative to NMR.

The spatial imaging of spins in a sample (electrons or nuclei) can be achieved by employing either Continuous Wave (CW) or pulsed spectroscopic excitation and detection methods along with magnetic field gradients that spatially encode the magnetic resonance signals.[17,28] Until recently, most efforts in ESRI have been directed towards the observation of large biological subjects[4,43–45] with the main purpose of determining

the radical and oxygen concentrations (by its effect on the radical line width). Such experiments, conducted in vivo, employ low fields of ~10 mT at low electromagnetic (EM) frequencies (which results in relatively low spin sensitivity), so that the EM energy will penetrate deeply into the biological object. Consequently, a typical voxel resolution in low-frequency ESR experiments is ca. 2 mm$^3$. Most low-field ESRI techniques are based on CW detection where the image is obtained by applying static gradients in various directions with respect to the object (the so-called back projection technique). However, a single pulse Free Induction Decay (FID) sequence in conjunction with static magnetic field gradients is sometimes used.[45]

Whereas in-vivo ESRI of small animals requires working at low frequencies, ESRI directed towards microscopy can and should be employed at higher frequencies for reasons of improved sensitivity and resolution. Prior to our recent work,[16,19,46,47] experiments in ESR microscopy (ESRM) were scarce, mainly due to major technological difficulties, and the lack of appropriate paramagnetic probes to image. Thus, for example, CW detection in conjunction with the modulated field gradients (MFG) method was used to spatially encode the signals, obtained at a resolution of ~10 μm in 1D,[48,49] whereas 2D images exhibit resolution of ~100 μm$^2$.[50] The CW technique with static magnetic field gradients (where the image is obtained by the Projection Reconstruction, PR, method[17]) achieved a resolution of ~10 μm for 1D experiments,[51] and 2D/3D resolution of the order of ~100–200 μm$^2$.[17] These earlier results are not as good as our recent work,[19,46] which achieved a resolution of ~10 × 10 × 30 μm in 45 min of acquisition, by CW imaging.

Pulsed ESRM is more challenging than CW since it requires fast gradient switching and spin probes with sufficiently long $T_2$'s.[39,52–55] Thus, previous work in high-resolution pulsed ESRM was mainly conducted with a unique organic conductor crystal termed (FA)$_2$X, which has a very long $T_2$ of ~6 μs at room temperature. With this material, 1D imaging with ~10 μm resolution was reported in a pulsed X-band (9 GHz) study.[56] Low-frequency pulsed RF ESR, employing a standard NMR microscopy gradient system, achieved 3D images with a resolution of ~[20–30 μm]$^3$ [55,57] after ~10 hours of data acquisition. The unique crystals used in these experiments and the long acquisition times are not attractive for biological, biophysical, and most materials science applications. Again, note for comparison our recent pulsed ESRM results (described below), which demonstrated with a high spin concentration sample a measured resolution of ~3 × 3 × 8 μm after 25 min of acquisition.[16,47]

## IMPROVEMENT OF SENSITIVITY AND RESOLUTION

Following this short background and a "snapshot" of our recent capabilities vs. the previous efforts in the field of ESRM, we will now describe in more detail how this improvement was achieved and further can be done in the future. The intuitive approach to improve the sensitivity and image resolution is to reduce the size of the detection/imaging probe. In NMR this implies the use of microcoils, which indeed enabled the most sensitive and high-resolution induction detection experiments to date.[15,18] In ESR microcoils do exist but, due to the higher RF frequencies involved, it is far more beneficial to employ resonant structures with higher $Q$ (~1000 vs. ~10 of the microcoils). In addition, at high frequencies it is much easier to couple the energy in and out of a resonant structure than a microcoil.[58] The downside of work with resonant structures is that unlike microcoils, their size is dictated by the microwave wavelength. One way around this problem is to use loop-gap resonators, which in principle can be manufactured with arbitrary dimensions; however in practice, at high frequencies, their $Q$-factor and size are limited.[59] Another possibility of reducing the resonant structure dimensions is to employ high permittivity materials (where the wavelength is much smaller than in free space) in its construction. This is the approach we chose, which resulted in a dramatic decrease of the resonator size vs. similar metallic structures, while maintaining relatively high $Q$. The downside of this approach is that one must rely upon a limited set of available materials (in terms of their electromagnetic properties). However, such high permittivity/high $Q$ materials are also very useful for the telecommunication industry, so this field is in constant development and new high permittivity materials may be produced in the future.[60–62]

**ESR Signal:** We now provide a more quantitative analysis of the sensitivity and image resolution in ESR experiments, starting with the CW mode: The Signal-to-Noise-Ratio (SNR) in a CW experiment is given by:[19]

$$SNR_{CW} \approx \frac{\chi_0'' V_v Q_u \sqrt{P}}{8 V_c \sqrt{k_b T \Delta f}} \cdot \frac{1}{1 + (Q_u \mu_0 / 2 V_c \omega_0) P \gamma^2 T_1 T_2} \quad (1)$$

where $\chi_0''$ is the resonant magnetic susceptibility of the sample (per unit of volume), $Q_u$ is the unloaded quality factor of the resonator, $\mu_0$ is the free space permeability, and $P$ is the incident MW power. The sample volume is given by $V_v$, and the resonator effective volume[19] is $V_c$. The rest of the parameters in eq 1 are Boltzmann's constant ($k_b$), the electron gyromagnetic ratio ($\gamma$), the temperature ($T$), the detection bandwidth ($\Delta f$), the MW frequency ($\omega_0$), and the relaxation times of the spins

$(T_1, T_2)$. The maximum SNR is achieved (for medium power) when:[36]

$$(Q_u\mu_0 / 2V_c\omega_0)P\gamma^2 T_1 T_2 = 1/2 \qquad (2)$$

and then eq 1 can be written as:

$$
\begin{aligned}
SNR_{CW}^{optimal\ P} &\approx \frac{\chi_0'' V_v \sqrt{2Q_u}\sqrt{\omega_0}}{8\sqrt{2}\sqrt{\mu_0}\gamma\sqrt{T_1 T_2}\sqrt{V_c}\sqrt{k_b T\Delta f}}\frac{2}{3}\\
&\approx \frac{\mu_0 H_0 \chi''(\omega_0/\Delta\omega)V_v\sqrt{2Q_u}\sqrt{\omega_0}}{8\sqrt{2}\sqrt{\mu_0}\mu_0 H\gamma T_2\sqrt{V_c}\sqrt{k_b T\Delta f}}\frac{2}{3}\\
&\approx \frac{\sqrt{2}\sqrt{2\mu_0}M\omega_0 V_v}{24\sqrt{V_c}\sqrt{k_b T\Delta f}}\sqrt{\frac{Q_u}{\omega_0}}
\end{aligned}
\qquad (3)
$$

Here $M$ is the magnetization of the sample, as given by the Curie law,[63] and $H_0$ is the static magnetic field. The derivation here used the optimal $P$ from eq 2. Furthermore, both the numerator and the denominator were multiplied by $\mu_0 H$ while considering the fact that the resonant susceptibility, $\chi_0''$, is related to the static susceptibility, $\chi''$, through $\chi_0'' = \chi''(\omega_0/\Delta\omega)$ (where $\Delta\omega$ is the line width, which is $\sim 2/T_2$). In addition, it was also assumed, for simplicity, that $T_1 = T_2$.

The SNR of a sample with a volume $V_v$ in a pulsed ESR experiment is given by an expression similar to that derived for the CW case, with equivalent approximations (up to a constant):[19]

$$SNR_{pulse} \approx \frac{\sqrt{2}\sqrt{2\mu_0}MV_v\omega_0}{16\sqrt{V_c}\sqrt{k_b T\Delta f}}\sqrt{\frac{Q_u}{\omega_0}} \qquad (4)$$

All the parameters in this equation were described in relation to eq 1. From eqs 3 and 4 it is apparent that the voxel SNR, both in the CW and the pulse cases, is proportional to $\omega_0^{1.5}/\sqrt{V_c}$ (since $M$ is linear with frequency, for the Curie law). Therefore, in order to improve the voxel SNR, one has to decrease the resonator size as much as possible and/or employ higher frequency.

**Magnetic Field Gradients:** In many applications, where the sample is inhomogeneous, a high spin sensitivity is not enough, and one is also interested in obtaining spatially resolved magnetic resonance information. The most effective method to acquire this information is to apply magnetic field gradients over the sample by means of gradient coils. The stronger the gradients are, the better the spatial resolution will be. Therefore, again, the intuitive approach is to try and minimize the size of the gradient coils and thereby to increase the magnitude of the gradients. These arguments can be presented in a more quantitative manner: With CW detection, one can employ either the MFG or the PR imaging method (see above). In the MFG method the image resolution is given by:[48]
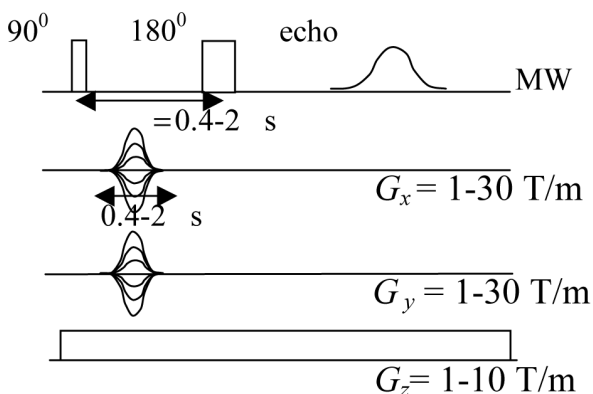
$$\Delta z = 2\Delta B_{1/2}/G_z \qquad (5)$$

Fig. 1. Typical pulse imaging sequence employed in ESRM. Phase gradients shaped as "half sinus" wave are used for spatially encoding the $x$ and $y$-axes of the sample, while a constant gradient is used along the $z$-axis. Typical peak values of the pulsed ($G_x$, $G_y$) and the constant ($G_z$) field gradients are shown. (See also refs 16,19 for more details.)

Thus, for a radical with line width of $\Delta B_{1/2} = 0.01$ mT (which is a typical value for trityl radical[64]), a gradient of $G_z \sim 20$ T/m, corresponds to 1 μm resolution. Similar gradient values are required for the PR method (within a factor of 2).[17] For the small-scale imaging probes we employ, achieving such gradients is not considered a major technological challenge, since we already achieved a CW gradients of more than 5 T/m with a relatively large 9 GHz imaging probe.[16,46,47]

With pulse detection and pulsed field gradients the effectiveness of the gradients is closely related to the imaging sequence employed. When choosing an imaging sequence suitable for pulsed ESR, one is faced with many constraints that do not exist for NMR imaging. For example, shaped excitation pulses, used for slice selection, are difficult to realize with microwaves on a sub-microsecond timescale. In addition, short rectangular gradient pulses with sharp edges are also difficult to achieve.[53,54] The simple sequence shown in Fig. 1 avoids most of these difficulties[16,28,55] and was used in our recent pulse experiments. Considering this sequence, we can write that for a radical with a Lorentzian line shape of width $1/(\pi T_2)$, the constant gradient ($G_z$ in Fig. 1) should satisfy the condition:[56]

$$G_z = 2/\gamma\Delta z T_2 \qquad (6)$$

In order to obtain spatial resolution of at least $\Delta z \sim 5$ μm along the z-axis of the sample, the gradient $G_z$ should be $\sim 2$ T/m (for $1/(\pi T_2) = 0.28$ MHz), which is readily available.[16,47] It should be noted that applying this gradient throughout the signal acquisition period does not significantly affect the echo amplitude (contrast to NMR, where the maximum applied gradient is limited by this

phenomena). This advantage of ESRM is apparent after reviewing the equation:[28]

$$Echo\ Amplitude = e^{(-\frac{1}{3}\gamma^2 G_z^2 D\tau^3)} \qquad [7]$$

Employing eq 7 even with diffusion coefficient of $D = 10^{-9}$ m$^2$/s, a very high $G_z$ of 40 T/m and $\tau = 1$ μs (Fig. 1), results in an echo decay of only ~2%. Thus, clearly even with gradients that correspond to sub-micron image resolution, there is no significant prohibiting decay from diffusion. Nevertheless, as described in the next section, in some applications we will be interested in exploiting the effect of echo decay under large gradients in order to obtain the self-diffusion coefficient of the imaged radicals in various parts of the sample, which NMR imaging achieves so well (but with lower resolution).[28] Such measurements could be performed in ESRM by means of a stimulated echo sequence, taking advantage of the relatively long $T_1$ with respect to $T_2$ (in most radicals).[65] For such a sequence, the argument of the exponent of eq 7 features not $\tau^3$ but $\sim T_1 \cdot \tau^2$.[65] This substitution leads to an attenuation of ~15% (for $T_1 = 10$ μs and the parameters $\tau$, $D$, $G_z$, as considered above), and thus for the stimulated echo sequence any slight increase in $\tau$ and/or $G_z$ will definitely lead to pronounced echo decay effects, which will enable the acquisition of diffusion-weighted images when necessary.[28,66]

From the constant $z$-gradient, we now turn to the $x$- and $y$-phase gradients (Fig. 1). These gradients should satisfy the condition:[28]

$$\int_t G_x dt = \frac{1}{(\gamma/\pi)\Delta x} \qquad (8)$$

It is clear from this expression that the shape of the phase gradient is not of importance, thereby relaxing the technical constraints for its generation. We have already demonstrated the operation of such phase gradients with duration of ~0.7 μs, and with peak value of $G_x$ ~26 T/m, which corresponds to ~3 μm resolution.[47]

## EXPERIMENTAL RESULTS

Having formulated the governing equations in terms of sensitivity and resolution, both for CW and pulsed detection methods, we now describe briefly some of our recent experimental results conducted at 9 and 16 GHz.[16,19,46,47] These experiments not only validated our calculations, but can also be used to estimate what is achievable at higher magnetic fields. Our CW and pulsed ESRM system architectures were described in detail,[16,46] and we shall not repeat this description here. The imaging probe, which is the key component of the system, was recently modified to operate at 16 GHz in pulse mode, and its schematic drawing and description is given in Fig. 2. The microwave resonant structure is based on SrTiO$_3$ or TiO$_2$ single crystals machined to a cylindrical shape with a diameter of 1.4 or 2.05 mm, respectively. The gradient coils are arranged on a



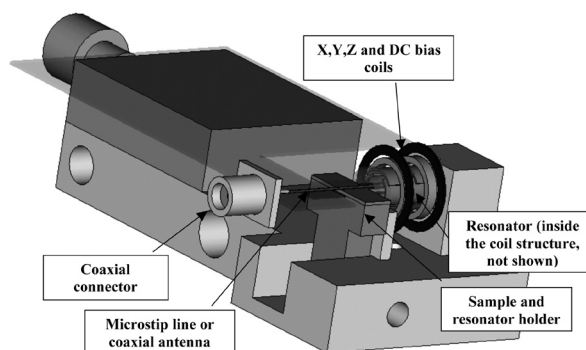Fig. 2. A schematic drawing of the 16 GHz pulse imaging probe.

4.6 mm o.d. cylinder covered with a thin (0.2 μm) gold layer that shields the microwave resonators but enables penetration of the pulsed magnetic field gradients. A DC bias coil is used to compensate for the static magnetic field drifts (by means of a field frequency lock mechanism[16]). Using this probe we were able to obtain 3D pulsed ESR images with a resolution of ~3 × 3 × 8 μm after 25 min of acquisition employing a high spin concentration sample (Fig. 3), and a resolution of ~7 × 7 × 12 μm with a sample containing a low concentration of trityl radical in solution (Fig. 4). The spin sensitivity in these experiments was ~10$^7$ spins for one hour of signal averaging, which is in agreement with our theoretical predictions.[16,47] The 16 GHz probe was also employed recently to obtain $T_2$-resolved 3D images of biodegradable microspheres embedded in trityl solution.[47]

Another type of spatially resolved information is the ESR spectrum for each voxel. Such information can be obtained both by pulse and by CW techniques. Figure 5 shows an example of spectral-spatial imaging with CW detection, which provides high-resolution spatially-resolved ESR spectra.

## FUTURE TRENDS AND ESR NANOSCOPY

Based on our theoretical analysis and the experimental results,[16,19,46,47] we can predict that this technology could achieve, at room temperature, a resolution of ~1.5 × 1.5 × 10 μm after a few minutes of acquisition, with CW detection at a frequency of 60 GHz. By employing pulse detection at 60 GHz, we expect to achieve a resolution better than ~1 × 1 × 5 μm in ~10 min of acquisition, for 1mM trityl solution. Extrapolation beyond 60 GHz is questionable, since at higher frequencies the current resonator design (see Fig. 2) becomes too small to handle, the microwave technology is more limited in terms of the availability of low loss components, and simple electromagnets can no longer be used.

The experiments described above were directed at measurements of biologically related samples. Therefore they are appropriately carried out only around
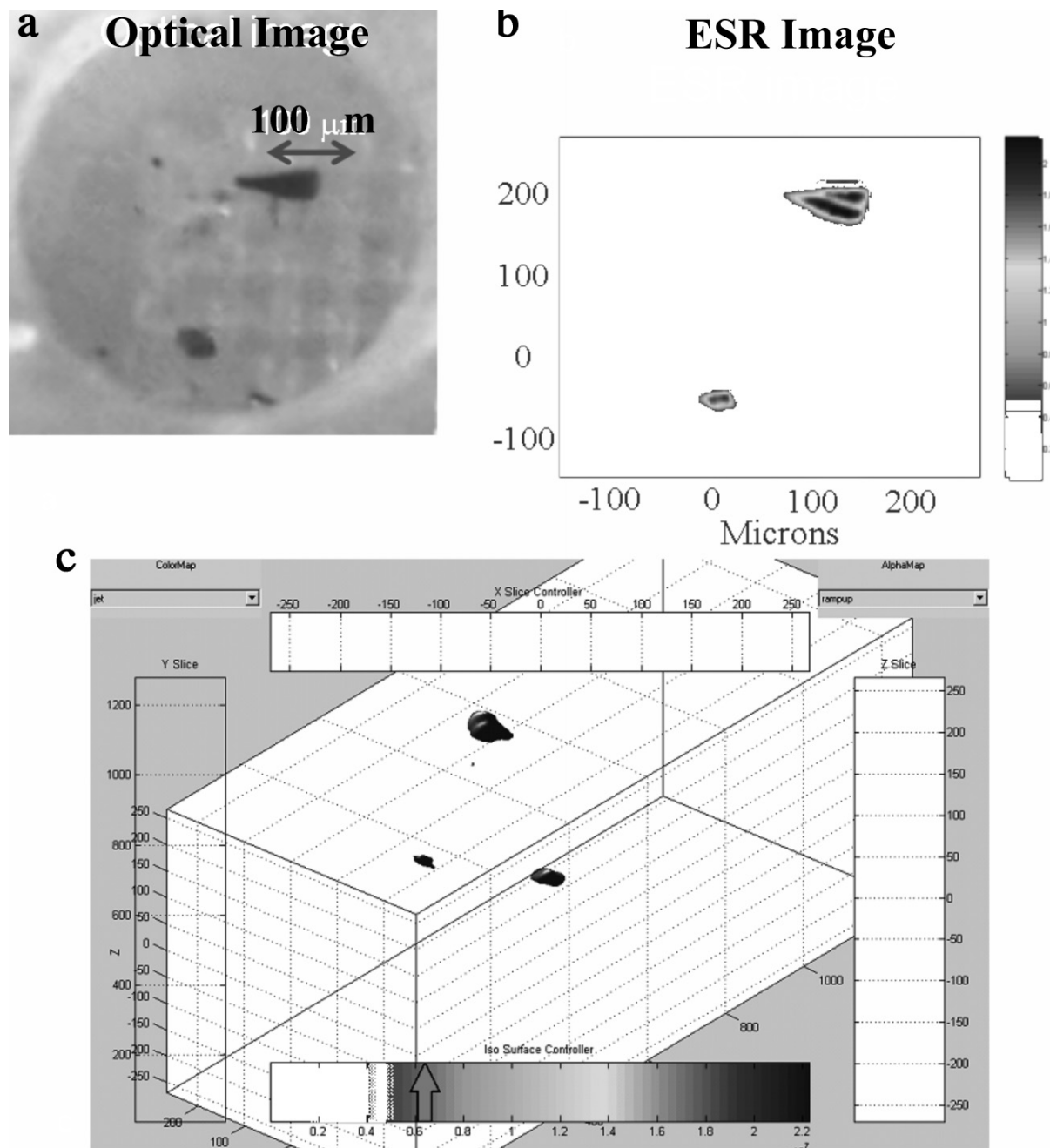
Fig. 3. Optical and pulsed ESR images of a test sample made of 3 small crystals of LiPc. (a) An optical image of the crystals shown through the hole in the cylindrical dielectric resonator we employ[16] (the third crystal is partially hidden). (b) A 2D cut of the 3D ESR image obtained at 16 GHz. (c) 3D object reconstruction based on the 3D ESR image data. (The third, smallest crystal is positioned at a different $z$-plane and thus not apparent in the 2D cut, but can be seen in the full 3D data.)

room temperature and with modest acquisition times of up to about an hour. However, many applications, especially in the field of materials science, can "tolerate" much lower temperatures and longer acquisition times. It is therefore worthwhile to look into the possibility of employing the high permittivity resonators described above at cryogenic temperatures and in conjunction with long measurement times. Of course, imposing a low temperature as a measurement restriction limits the "generality" of our approach. Nevertheless, it can provide a significant payoff. Needless to say, at low temperatures the additional advantages of induction
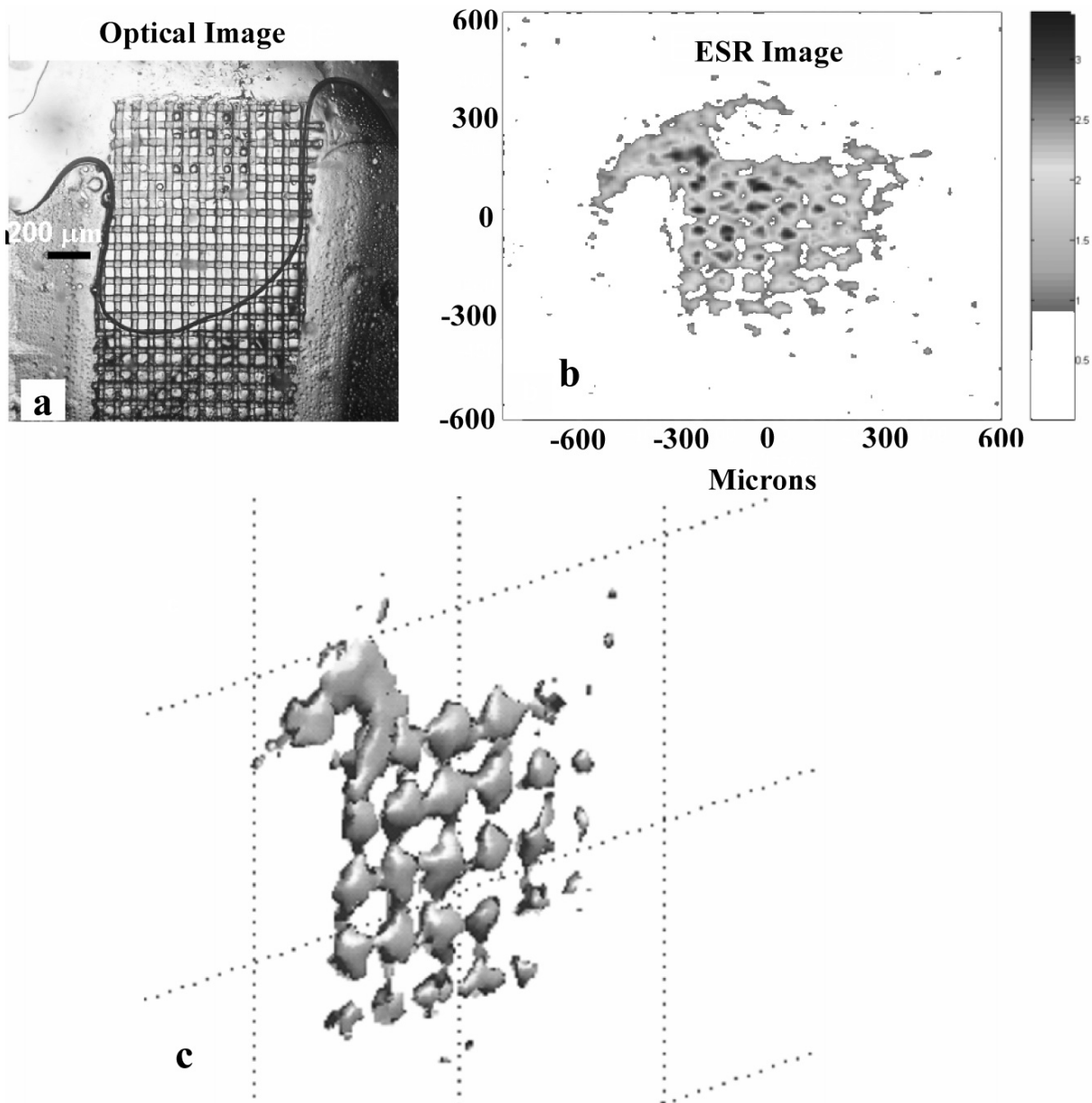
## Optical Image

## ESR Image

Fig. 4. Optical and pulsed ESR images of a test sample made of 1mM trityl radical water solution[134] embedded in a woven nylon mesh with mesh aperture of $50 \times 50$ μm and wire diameter of 39 μm (Goodfellow, USA).[47] (a) An optical image of the solution and the mesh prior to measuring the ESR image. (b) A 2D cut of the 3D ESR image obtained at 16 GHz. (c) 3D object reconstruction based on the 3D ESR image data. The discrepancies between the ESR image and the optical image are due to sample dehydration during the ESR measurements.

detection, as mentioned above (spectroscopic capability, simple sample preparation, and parallel 3D image collection), are still valid.

A potential problem related to the use of high permittivity dielectric resonators of the type employed here, instead of microcoils or other metallic structures, is that their dielectric properties strongly depend upon the frequency of operation and the temperature. Luckily, there is a wealth of information in the literature about the two single crystals we are currently using ($SrTiO_3$ and $TiO_2$).[60,61,67,68] This enables one to estimate the real part of the permittivity and the quality factor at differ-
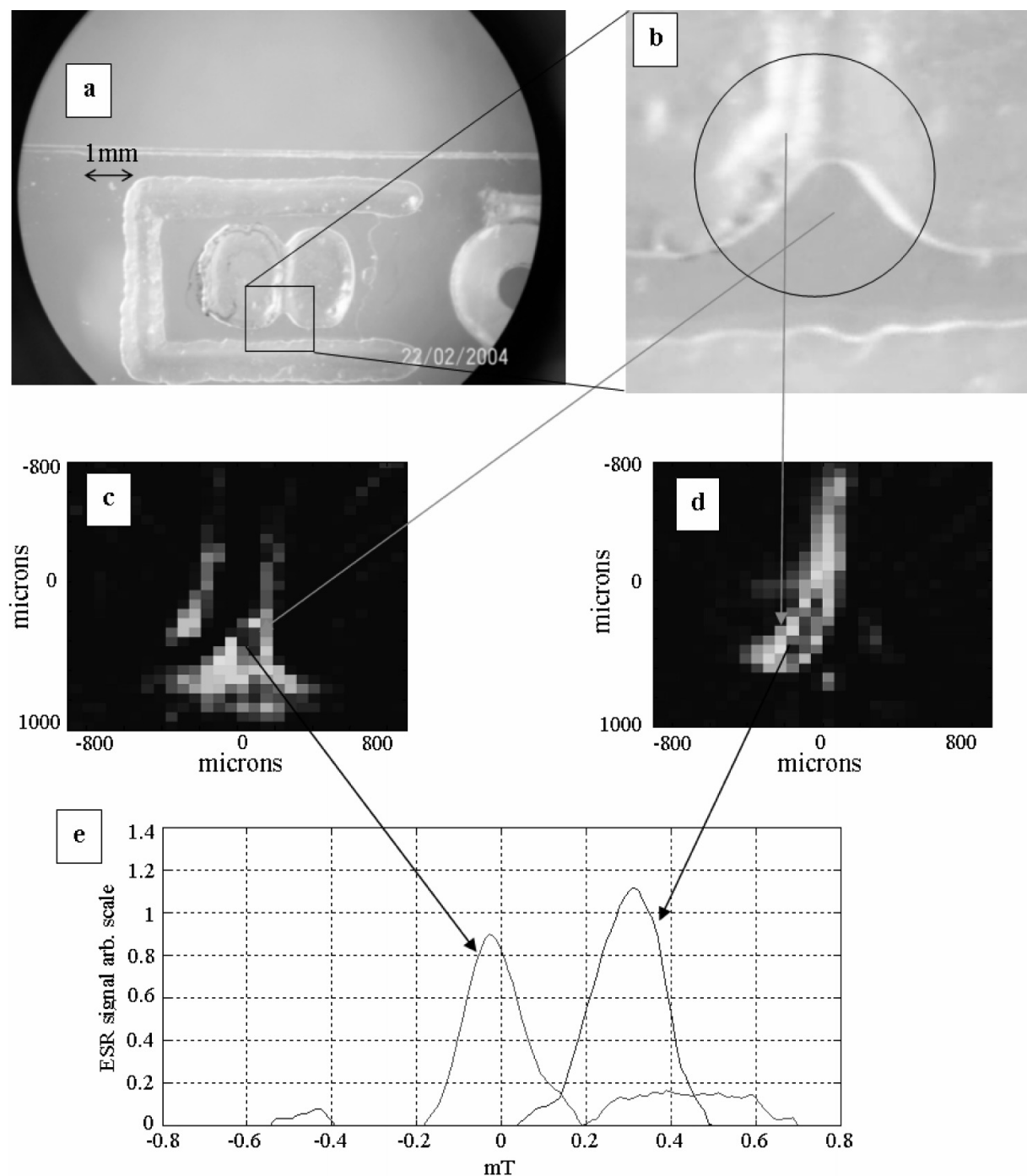
Fig. 5. Example for spectral-spatial image obtained with the 9 GHz CW ESR microscope. a. Optical image of the sample made of trityl solution and solid LiNc-BuO (dark traces left after evaporation). b. Closer look at the area that was imaged inside the resonator effective volume (superimposed circle). c. ESR image of the trityl obtained by taking only the part in the spectrum where the trityl is dominant. d. The same as c but for the LiNc-BuO. e. ESR spectrum obtained with the spectral-spatial algorithm at two points as marked by the arrows, corresponding to the spectrum of the trityl solution (left peak) and the solid LiNc-BuO.

ent temperatures and frequencies, as shown in Fig. 6. The information in Fig. 6 can be used to calculate the linear dimensions of the resonator, which are inversely proportional to the frequency and $\sqrt{\varepsilon}$. The calculated

resonator volume, $V_c$, along with its quality factor (as obtained directly from Fig. 6), can be inserted into eq 4 to obtain the SNR for a given radical $T_2$ ($\Delta f = 1/\pi T_2$). Figure 7 shows the SNR results as obtained with these
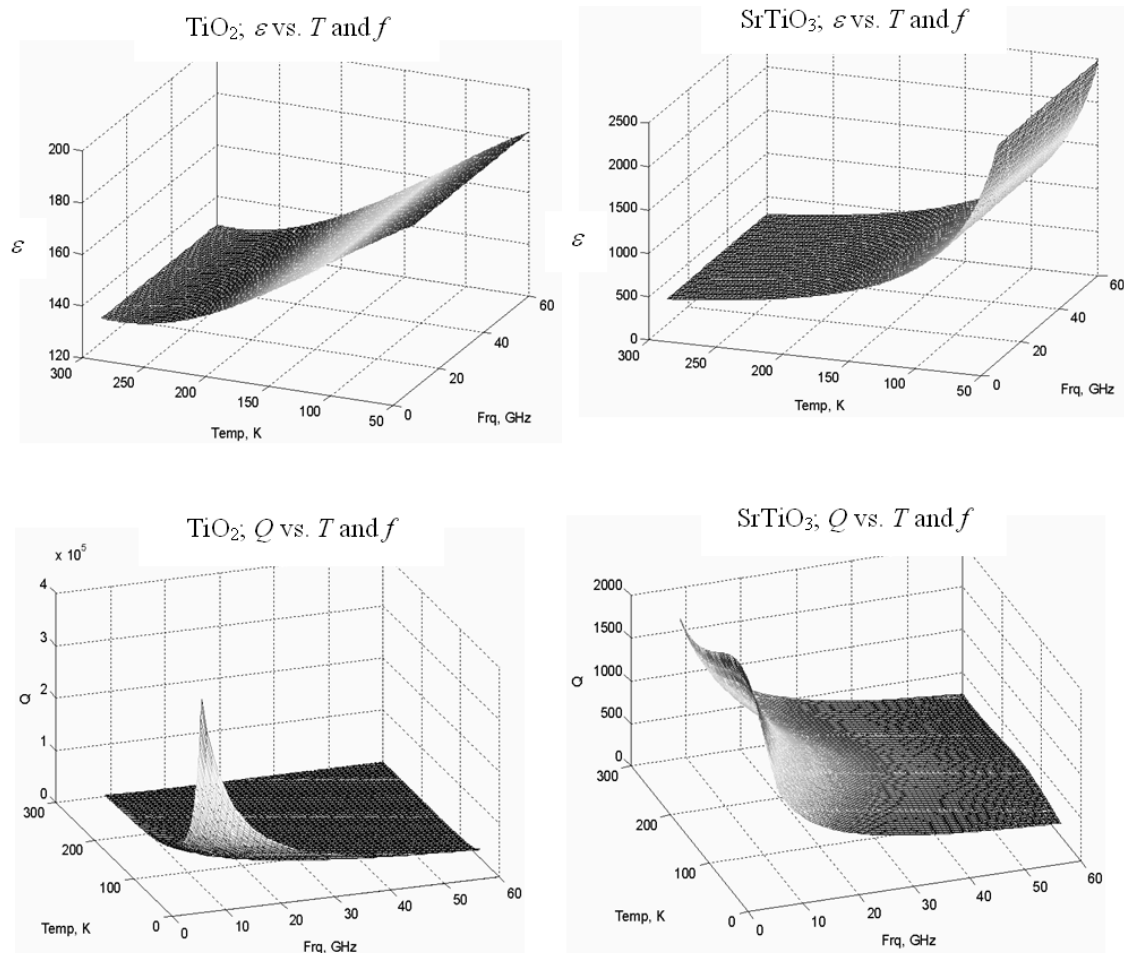
TiO$_2$; $\varepsilon$ vs. $T$ and $f$

SrTiO$_3$; $\varepsilon$ vs. $T$ and $f$

TiO$_2$; $Q$ vs. $T$ and $f$

SrTiO$_3$; $Q$ vs. $T$ and $f$

Fig. 6. The calculated permittivity ($\varepsilon$) and $Q$ of SrTiO$_3$ and TiO$_2$ single crystals vs. temperature and frequency.

calculations, assuming radical having $T_2$ of 2.5 μs and $T_1$ of 13 μs. The $T_1$ is relevant (although it is not explicitly included in eq 4) since we assume averaging with a $1/T_1$ repetition rate; (thus in 60 min one can reach up to ~276 M acquisitions that improve the single shot SNR by a factor of ~16,600). It can be seen that at a frequency of 60 GHz and 50 K, one approaches a sensitivity of 1000 electron spins for 1 hour of acquisition. Above 60 GHz and below 50 K the available information is not reliable enough to safely extrapolate the SNR calculations with a reasonable degree of certainty.

The improved sensitivity at higher frequency and at lower temperatures can be accompanied by a corresponding improvement in image resolution. For example, at 60 GHz the diameter of the TiO$_2$ probe would be only ~0.6 mm. The small resonator size would en-

able one to reduce the distance between the gradient coils and the sample to ~1.2 mm. This would increase the available peak gradients by more than a factor of 4 with respect to the present 16 GHz probe. Such an improvement, combined with the use of 1000-V sources for the gradient current drivers (vs. 400 V in the present configuration), and employing radicals having long $T_2$'s at low temperatures, would lead to an image resolution better than 100 nm (see eq 8 and Fig. 1).

### POSSIBLE APPLICATIONS

We have seen that ESR microscopy at room temperature is already available with micron-scale resolution and can be expected to reach the submicron level in the near future. In addition, it was shown that ESR nanoscopy at low temperatures is feasible and our efforts in this direc-
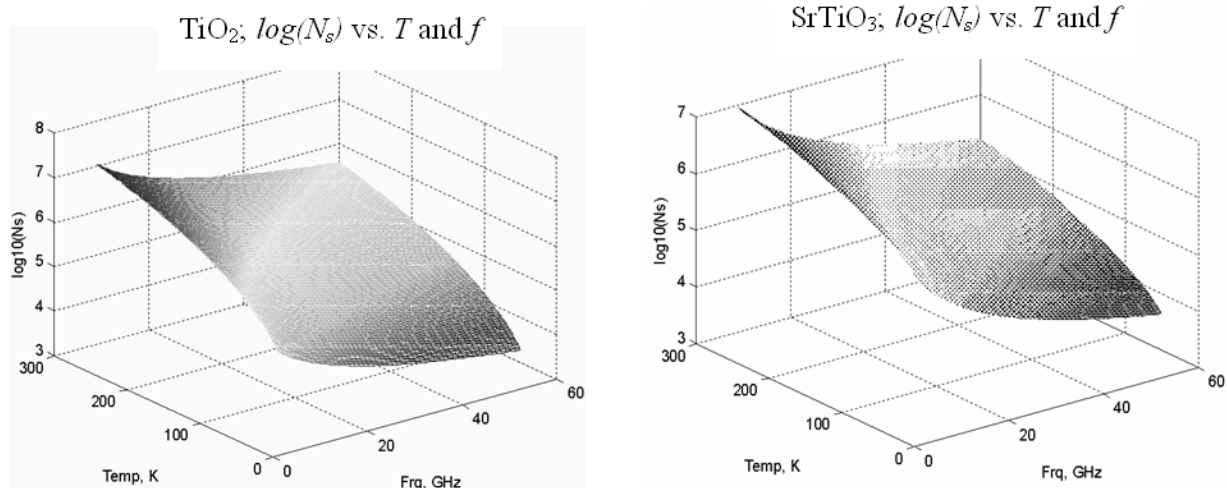
TiO$_2$; $log(N_s)$ vs. $T$ and $f$

SrTiO$_3$; $log(N_s)$ vs. $T$ and $f$

Fig. 7. The calculated minimum number of detectable electron spins by pulsed ESRM after 60 min of of acquisition (*Ns*), employing resonators based on SrTiO$_3$ and TiO$_2$ single crystals vs. temperature and frequency.

tion have already begun. The question that still remains to be answered is what are the applications for which such new capabilities can be useful? Below we will try to provide at least a partial answer for this fundamentally important aspect of the research.

*ESR microscopy*

When fully developed, ESRM can have substantial benefits mainly for biological and medical research. Here we provide some representative examples that reflect on the broad influence that this method may have in the near future.

*a. Applications by analogy to NMR microscopy.*Some of the potential applications of ESRM can be appreciated by relating it to a conceptually similar NMR microscopy histological device that examines biological specimens, in vitro or ex vivo.[28,29,69] This technique, despite its resolution limitation (i.e., ~10–20 mm$^3$, as described above) has found many applications in bio-sciences, such as the imaging of biophysical processes in plants, tissues, and live unicellular organisms.[31–34,66,70] Recently a combined NMR–optical microscope was demonstrated, that tries to benefit from the relative advantages of each methodology and provides more complete sample information.[32] Nevertheless, all these efforts resulted in limited success, mainly due to the resolution limitations and the relatively long acquisition times of NMR microscopy. A comparable ESRM technology, examining samples "dyed" with free radicals, would have the advantages and capabilities of the NMR microscope, and could be applied to similar cases but with an order of magnitude of resolution improvement with respect to all 3 axes and the ability to observe much

lower spin concentration. In addition, the high sensitivity of the ESR line shape to dynamic effects can enhance the possible range of image contrast parameters.

*b. Controlled drug release.* Recently, there has been extensive use of polymeric microspheres as a matrix for the slow release of drugs in the body.[71] To control this process, one requires tools for observing the drug distribution within the sphere, after preparation, and during the release process. Currently the major tool used for such monitoring is laser scanning confocal fluorescence microscopy, with fluorescent-labeled drugs. The problems with this method are that it cannot penetrate deep into the sphere, it provides non-linear image intensity (due to unknown absorption and scattering coefficients in the sphere), and it cannot be employed during the in-vitro/in-vivo release process.[72] Furthermore, fluorescence does not have a good capability to quantify the porosity of the spheres and the self-diffusion coefficients of the molecules in the sphere. By attaching a spin label to the drug, this process can be monitored in a 3D manner with ESRM techniques to provide the time-resolved drug distribution in the microsphere, the sphere's porosity, and information about the drug molecular self-diffusion and rotational correlation time. More details about ESRM and the monitoring of slow release, along with initial experimental results, are given in our recent publication.[47]

*c. Measurements of oxygen partial pressure (pO$_2$) in model systems and living cells.*[44] The concentration of oxygen is one of the most important variables in many physiological, pathological, and therapeutic

processes. As the terminal acceptor in the electron transport chain, $O_2$ plays a critical role in cellular metabolism and in reperfusion poisoning.[73] There is an increasing recognition that accurate measurement of $O_2$ concentration would enable one to enhance the basic understanding of many types of physiological phenomena at both a general and specific level.[74] Although many efforts have been made in this direction with NMR and fluorescence techniques, they all have their limitations. For example, NMR has limited $O_2$ sensitivity and low resolution, while fluorescence probes have the problem of photo-toxicity, have good $O_2$ sensitivity only at very low $O_2$ concentrations, and require careful calibration of temperature and local viscosity to obtain accurate results.[75,76] ESR, which measures $O_2$ concentration via its effect on the line width of the radical probe, has capabilities that are complementary, or, with the new microscope, superior to these methods.[75,77,78] The introduction of an ESRM technique will enable in vitro/ex vivo high-resolution examination of living cells, in the cellular and subcellular level (see below), which could provide more insight in research on cellular and overall tissue biophysiology. Such ESRM results could also be correlated with "large scale" in vivo animal and human measurements.

*d. Imaging model membranes and membranes in live cells.* Extensive research indicates the existence of different phase domains within the cell membrane (often called membrane "rafts"), in which key membrane proteins tend to reside. Such domains, rich in cholesterol and sphingolipids, have implications for a number of important membrane functions. They can be small (nm scale) with a short lifetime (μs scale) or can be larger (μm scale) and stabilized to reach a "lifetime" of several minutes (by liganded and oligomerized receptor molecules).[79–81] Direct imaging of the domain separation phenomenon was obtained so far only by means of 3D fluorescence imaging with unique model membranes (Giant Unilamellar Vesicles, GUVs) "designed" to exhibit such phase partition behavior.[82,83] The fluorescent probes, which do not exhibit different "spectra" for the different phase domains, had to be "engineered" to partition only into one of the artificial membrane phases. This problem, as well as the possible limited sizes of these domains, has currently prohibited the direct observation of such phenomena in live cells. ESR is very useful in identifying the existence of different phase domains using spin-labeled lipids (partitioning to both membrane phases), which exhibit different spectra for the different membrane phases in membrane vesicles[80,84] and recently also in live cells.[85] ESRM can thus bridge the gap between the conventional macroscopic ESR measurements to the microscopic nature of domain phenomena and thus may enable direct observation of phase separation in GUVs, patterned lipid bilayers,[86] and possibly even in live cells.

*e. Imaging of radiation effects.* ESRI has been used for a long time in dosimetry and for the assessment of radiation damage in bones[87] and tooth enamel.[88] It is probably the only analytical tool that can be used for this purpose. In order to accurately estimate the radiation dosage, one should measure the spin *concentration* (which can be fairly inhomogeneous), rather than the more common signal amplitude measurements (which are hard to calibrate). Improved spatial resolution and sensitivity would reveal the effects of ionizing radiation on a fine scale, which is of special interest in this research area.[89,90] For example, with ESRM one may differentiate between situations where a single intense radiation particle created the same amount of paramagnetic centers as created by several much weaker particles (and then of course, the first case may prove to be more dangerous in terms of its radiation effects). These two cases are indistinguishable with bulk ESR measurements or with low-resolution imaging.

*f. Imaging of reactive oxygen species (ROS).* The observation of ROS by means of low resolution in-vivo ESR measurements is a well-established method.[91–95] One manner of doing so is to introduce stable spin probes into the sample and to observe the reduction of the ESR signal in various parts of the sample due to chemical reaction with the reactive species. This was done in the past with nitroxide-type spin probes,[96,97] and recently also with trityl radical, and its derivatives.[98] Another approach is to employ spin traps that "capture" the short-lived ROS and generate stable free radicals, whose signal can be observed in the areas where the reactive species are born.[92] Previous efforts did not provide high enough resolution, and therefore the exact location of the radical generation centers and their relation to antioxidant effects are still unclear. Such information (which can be measured in vitro by ESRM) would help to understand the mechanism of radical generation, which is of prime importance to issues such as diabetes, ulcers, and antioxidant therapy.[93]

*g. ESRM of cancerous tissues.* Recently, stable microparticulates of lithium naphthalocyanine-type (LiNc-BuO) radicals[99] were implanted in animals and were used over long periods of time (weeks) to measure $pO_2$ in cancerous tissues in vivo. Here in vitro ESR microscopy is essential to complete the picture by providing information about the radical distribution at the extra- and intracellular level. This will enable one to verify the internalization of the radicals inside the

cells and also to correlate the low-resolution in vivo $pO_2$ measurements with the actual $pO_2$ levels inside the cell (for example, in the nucleus).

*h. Other types of possible ESRM applications.* These include the less explored aspects of ESR, such as the measurements of microviscosity,[100] pH,[101] redox state,[102] charge and potential, polarity (hydrophilicity), and the identification of thiol groups.[103,104]

*i. ESRM vs. fluorescence techniques.* Fluorescence methods are now routinely employed to observe biochemical reactions and processes within *living* cell cultures at high resolution.[105,106] ESRM at room temperature would not have quite as good resolution as fluorescence achieves (~1–2 μm against ~0.3 μm optical resolution) and its acquisition times are longer (typically several minutes against several seconds). Nevertheless it still could address many important aspects not accessible by fluorescence probes. These include, for example: measurements of flow and transport in three dimensions;[28] measurement of self-diffusion for various isotropic and anisotropic media in the cell;[28,66] accurate $pO_2$ imaging;[78] high specificity in superoxide imaging;[98] 3D measurements in non-transparent samples with accurate intensity information per voxel (3D fluorescence is difficult to calibrate due to uncertainties in extinction coefficient and scattering phenomena); measurements of a variety of image contrasts such as ESR relaxation times ($T_1$ and $T_2$); chemical specificity for many important reactions involving radicals;[91–93] possibility to correlate in-vitro with large-scale in-vivo measurements; and measurements at specific voxels of the ESR line shape, which provide information about various environmental/dynamic conditions.[107,108] This extensive information could be used in conjunction with a combined optical/ESR microscope (similar to the case of NMR microcopy with optical imaging[32]) to reveal many new aspects of the cellular riddle.

Other applications could be drawn from the wide literature on microscopy, but the bottom line is that ESRM is currently insufficiently developed: it certainly is not available commercially, and current technology provides the potential user with only limited resolution and sensitivity. We believe that the development of an adequate ESRM capability would likely stimulate additional applications, just as is often the case with the introduction of new technologies.

### ESR Nanoscopy

As described above, by lowering the temperature to ~77 K and raising the frequency to 60 GHz, a sensitivity of about 1000 electron spins, with spatial resolution of less than 100 nm should be achievable. These figures are currently based on theoretical estimates, yet to be supported by experimental evidence. Nevertheless, relevant studies are in progress, and it is legitimate to look ahead and inquire about the applications that can be pursued if/when this technology would achieve its goals. Currently we have identified two main fields that would benefit from such progress.

*a. Morphological and functional cell biology.* As described above, fluorescence microscopy provides unparalleled morphological and functional information in live cells, with a typical resolution ranging from 200 to 300 nm (for conventional "one-sided" microscopes), down to 100 nm (obtained with the new "4π microscopes").[109] With frozen bio-samples one can employ, for example, cryoelectron tomography to obtain 3D images with a resolution of ~5 nm, but only for samples that are thinner than ~1 μm.[110] Low-temperature ESR nanoscopy can bridge the gap between these two methods by providing 3D images, with a resolution better than 100 nm, of frozen bio-samples that are more than 100 μm in thickness. This can be done, for example, on live cells doped with soluble radicals or radical particulates, which are subsequently frozen rapidly and measured at low temperatures. Morphological information could be obtained by the imaging of such a radical "dye" that is well dispersed in the sample. Functional information can be obtained, for example, with a process involving ROS in a similar manner to what is done for live cells (see above), but at much higher resolution. Here the process will be stopped at a given time by freezing the cell, and an ultra-high-resolution "snapshot" of the ROS distribution at the time of freezing could be obtained.

*b. Semiconductor defects.* The operation principals of semiconductor devices are based upon the unique physical properties of the semiconductor material. These properties, such as the energy band structure and charge carriers' mobility, are very sensitive to crystal imperfections. Some imperfections in the form of "foreign" substitutional atoms are introduced deliberately, as in the case of the shallow donor- and acceptor-doped semiconductors. However, many crystal imperfections are unintentional and are due to non-optimal crystal growth techniques, device processing, and radiation-induced damage. In most cases such imperfections in relatively low concentrations do not significantly affect the mechanical properties of the semiconductor material, but dramatically change its electrical and optical properties.

In principle, detection of defects can be done either indirectly, through their effect on the physical/electrical

properties of the semiconductor, or directly by 3D structural imaging. The physical/electrical activity of the defects can be detected and characterized by techniques such as ESR,[111–115] NMR,[116–118] deep level transient spectroscopy,[119–121] and thermally stimulated current.[122,123] For large enough samples, these types of measurements can be used to detect even low densities of electrically active defects (introducing levels in the forbidden energy gap). However, this information, without the knowledge of the 3D defect distribution, is often insufficient. The structural nature of the defects can be characterized by methods such as transmission electron microscopy (TEM)[124–126] and various X-ray diffraction methods for detection of lattice imperfection.[127–130] The TEM technique provides excellent 2D resolution, but requires special sample preparation, and the interpretation of the results is often not straightforward. In addition, if the defects are sporadic and do not result in a relatively large ~1–2 nm crystal anomaly, they will not be detected.[126] X-ray diffraction techniques are also not sensitive to low defect densities, and can also produce only two-dimensional images. The low energy X-ray microscopy method (NEXAFS-SPXM) can be used to achieve 3D images with a resolution down to 10 nm, however, it works only in samples of relatively low atomic number, thickness of < 200 nm, and again, is sensitive only for major defects generating structural anomalies of at least several nm in size.[131–133]

Thus, it can be concluded that none of the current techniques can provide adequate 3D imaging of sporadic defects in conventional thick samples (1 micron and up), with deep sub-micron resolution. One should also point out that due to the nature of most defects (e.g., a single atom removed from the lattice at a certain point, with the nearest defect several angstroms away), the future prospects of direct structural imaging of such defects (requiring sub-angstrom resolution), are not very promising. ESR nanoscopy, which could detect the signal from such dispersed defects (assuming high enough sensitivity), and would be able to spatially resolve it from other defects in a resolution that can be better than 100 nm (depending on the magnetic field gradients employed), may become a very useful tool in this field.

## CONCLUSIONS

Magnetic resonance in general, and ESR in particular, has much to contribute to basic and applied science and technology. The new directions presented in this paper may very well be only the first step in a broad range of possibilities these fields still have to offer.

## REFERENCES AND NOTES

(1) Borbat, P.P.; Mchaourab, H.S.; Freed, J.H. *J. Am. Chem. Soc.* **2002**, *124*, 5304–5314.

(2) Breitmaier, E. *Structure Elucidation by NMR in Organic Chemistry: A Practical Guide*; Wiley: Chichester, West Sussex, England, 2002.

(3) Gadian, D.G. *NMR and its Applications to Living Systems*; Oxford University Press: Oxford, 1995.

(4) He, G.L.; Samouilov, A.; Kuppusamy, P.; Zweier, J.L. *Mol. Cell. Biochem.* **2002**, *234*, 359–367.

(5) Lindstrom, G.; Ahmed, M.; Albergo, S. et al. *Nuclear Instruments & Methods in Physics Research Section a-Accelerators Spectrometers Detectors and Associated Equipment* **2001**, *466*, 308–326.

(6) Twamley, J. *Phys. Rev. A* **2003**, *67*, 052318.

(7) Rabi, I. Nobel prize for *Nuclear magnetic resonance using atomic beam methods*. **1944**.

(8) Bloch, F.; Purcell, E.M. Nobel prize for *Nuclear magnetic resonance*. **1952**.

(9) Townes, C.H.; Basov, N.G.; Prokhorov, A.M. Nobel prize for *Maser and laser amplifiers (some of which are based on ESR)*. **1964**.

(10) Bloembergen, N.; Schawlow, A. Nobel prize for *The three level maser*. **1981**.

(11) Ernst, R.R. Nobel prize for *Development of the methodology of high resolution nuclear magnetic resonance (NMR) spectroscopy*. **1991**.

(12) Wuthrich, K. Nobel prize for *Nuclear magnetic resonance spectroscopy for determining the three-dimensional structure of biological macromolecules in solution*. **2002**.

(13) Lauterbur, P.C.; Mansfield, P. Nobel prize for *Discoveries concerning magnetic resonance imaging*. **2003**.

(14) Feynman, R.P., http://www.zyvex.com/nanotech/feynman.html **(1959)**.

(15) Ciobanu, L.; Seeber, D.A.; Pennington, C.H. *J. Magn. Reson.* **2002**, *158*, 178–182.

(16) Blank, A.; Dunnam, C.R.; Borbat, P.P.; Freed, J.H. *Appl. Phys. Lett.* **2004**, *85*, 5430–5432.

(17) Eaton, G.R.; Eaton, S.S.; Ohno, K. *EPR Imaging and in vivo EPR*; CRC Press: Boca Raton, FL, 1991.

(18) Glover, P.; Mansfield, P. *Rep. Prog. Phys.* **2002**, *65*, 1489–1511.

(19) Blank, A.; Dunnam, C.R.; Borbat, P.P.; Freed, J.H. *J. Magn. Reson.* **2003**, *165*, 116–127.

(20) Boero, G. Besse, P.A.; Popovic, R. *Appl. Phys. Lett.* **2001**, *79*, 1498–1500.

(21) Chao, S.H.; Dougherty, W.M.; Garbini, J.L.; Sidles, J.A. *Rev. Sci. Instrum.* **2004**, *75*, 1175–1181.

(22) Tsuji, S.; Masumizu, T.; Yoshinari, Y. *J. Magn. Reson.* **2004**, *167*, 211–220.

(23) Rugar, D.; Budakian, R.; Mamin, H.J.; Chui, B.W. *Nature* **2004**, *430*, 329–332.

(24) Manassen, Y.; Hamers, R.J.; Demuth, J.E.; Castellano, A.J. *Phys. Rev. Lett.* **1989**, *62*, 2531–2534.

(25) Durkan, C.; Welland, M.E. *Appl. Phys. Lett.* **2002**, *80*, 458–460.

(26) McDermott, R.; Trabesinger, A.H.; Muck, M.; Hahn, E.L.; Pines, A.; Clarke, J. *Science* **2002**, *295*, 2247–2249.

(27) Madsen, L.A.; Leskowitz, G.M.; Weitekamp, D.P. *Proc. Natl. Acad. Sci. USA* **2004**, *101*, 12804–12808.

(28) Callaghan, P.T., *Principles of Nuclear Magnetic Resonance Microscopy*; Oxford University Press: Oxford, 1991.

(29) Johnson, G.A.; Benveniste, H.; Black, R.D.; Hedlund, L.W.; Maronpot, R.R.; Smith, B.R. *Magn. Reson. Q.* **1993**, *9*, 1–30.

(30) Blumich, B. *NMR Imaging of Materials*; Oxford, Oxford University Press, 2000.

(31) Ishida, N.; Koizumi, M.; Kano, H. *Ann. Bot.* **2000**, *86*, 259–278.

(32) Majors, P.D.; Minard, K.R.; Ackerman, E.J., Holtom, G.R.; Hopkins, D.F.; Parkinson, C.I.; Weber, T.J.; Wind, R.A. *Rev. Sci. Instrum.* **2002**, *73*, 4329–4338.

(33) Ciobanu, L.; Webb, A.G.; Pennington, C.H. *Prog. Nucl. Magn. Reson. Spectrosc.* **2003**, *42*, 69–93.

(34) Ciobanu, L.; Pennington, C.H. *Solid State Nucl. Magn. Reson.* **2004**, *25*, 138–141.

(35) Gravina, S.; Cory, D.G. *J. Magn. Reson. Ser. B* **1994**, *104*, 53–61.

(36) Poole, C.P. *Electron Spin Resonance: A Comprehensive Treatise on Experimental Techniques*; New York, Wiley, 1983.

(37) Hornak, J.P.; Moscicki, J.K.; Schneider, D.J.; Freed, J.H. *J. Chem. Phys.* **1986**, *84*, 3387–3395.

(38) Moscicki, J.K.; Shin, Y.K.; Freed, J.H. *J. Magn. Reson.* **1989**, *84*, 554–572.

(39) Feintuch, A.; Tashma, T.; Grayevsky, A.; Gmeiner, J.; Dormann, E.; Kaplan, N. *J. Magn. Reson.* **2002**, *157*, 69–73.

(40) Blank, A.; Stavitski, E.; Levanon, H.; Gubaydullin, F. *Rev. Sci. Instrum.* **2003**, *74*, 2853–2859.

(41) Borbat, P.P.; Costa-Filho, A.J.; Earle, K.A.; Moscicki, J.K.; Freed, J.H. *Science* **2001**, *291*, 266–269.

(42) Freed, J.H. *Ann. Rev. Phys. Chem.* **2000**, *51*, 655–689.

(43) Eaton, G.R.; Eaton, S.S. *Concepts Magn. Reson.* **1995**, *7*, 49–67.

(44) Swartz, H.M.; Clarkson, R.B. *Phys. Med. Bio.* **1998**, *43*, 1957–1975.

(45) Yamada, K.I.; Murugesan, R.; Devasahayam, N., Cook, J.A.; Mitchell, J.B.; Subramanian, S.; Krishna, M.C. *J. Magn. Reson.* **2002**, *154*, 287–297.

(46) Blank, A.; Dunnam, C.R.; Borbat, P.P.; Freed, J.H. *Rev. Sci. Instrum.* **2004**, *75*, 3050–3061.

(47) Blank, A.; Freed, J.H.; Naraharisetti, P.K.; Wang, C.H. *J. Control. Release* **2006**, *III*, 174–184.

(48) Herrling, T.; Klimes, N.; Karthe, W.; Ewert, U.; Ebert, B. *J. Magn. Reson.* **1982**, *49*, 203–211.

(49) Herrling, T.; Fuchs, J.; Groth, N. *J. Magn. Reson.* **2002**, *154*, 6–14.

(50) Akademie Der Wissenschaften Der DDR, ZZG1 User manual. 1987.

(51) Karthe, W.; Wehrsdorfer, E. *J. Magn. Reson.* **1979**, *33*, 107–111.

(52) Milov, A.D.; Pusep, A.Y.; Dzuba, S.A.; Tsvetkov, Y.D. *Chem. Phys. Lett.* **1985**, 119, 421–425.

(53) Ewert, U.; Crepeau, R.H.; Dunnam, C.R.; Xu, D.J.; Lee, S.Y.; Freed, J.H.; *Chem. Phys. Lett.* **1991**, *184*, 25–33.

(54) Ewert, U.; Crepeau, R.H.; Lee, S.Y.; Dunnam, C.R.; Xu, D.J.; Freed, J.H. *Chem. Phys. Lett.* **1991**, *184*, 34–40.

(55) Feintuch, A.; Alexandrowicz, G.; Tashma, T.; Boasson, Y.; Grayevsky, A.; Kaplan, N. *J. Magn. Reson.* **2000**, *142*, 382–385.

(56) Maresch, G.G.; Mehring, M.; Emid, S. *Phys. B C* **1986**, *138*, 261–263.

(57) Coy, A.; Kaplan, N.; Callaghan, P.T. *J. Magn. Reson. Ser. A* **1996**, *121*, 201–205.

(58) Boero, G.; Bouterfas, M.; Massin C., Vincent, F.; Besse, P.A.; Popovic, R.S.; Schweiger, A. *Rev. Sci. Instrum.* **2003**, *74*, 4794–4798.

(59) Klug, C.S.; Camenisch, T.G.; Hubbell, W.L.; Hyde, J.S. *Biophys. J.* **2005**, *88*, 3641–3647.

(60) Krupka, J.; Geyer, R.G.; Kuhn, M.; Hinken, J.H. *IEEE Trans. Microwave Theory Techniques* **1994**, *42*, 1886–1890.

(61) Vendik, O.G.; Ter-Martirosyan, L.T.; Zubko, S.P. *J. Appl. Phys.* **1998**, *84*, 993–998.

(62) http://www.lsbu.ac.uk/dielectric-materials/

(63) Rinard, G.A.; Quine, R.W.; Song, R.T.; Eaton, G.R.; Eaton, S.S. *J. Magn. Reson.* **1999**, *140*, 69–83.

(64) Yong, L.; Harbridge, J.; Quine, R.W., Rinard, G.A.; Eaton, S.S.; Eaton, G.R.; Mailer, C.; Barth, E.; Halpern, H.J. *J. Magn. Reson.* **2001**, *152*, 156–161.

(65) Norwood, T.J. *J. Magn. Reson. Ser. A* **1993**, *103*, 258–267.

(66) Sehy, J.V.; Ackerman, J.J.H.; Neil, J.J. *Magn. Reson. Med.* **2001**, *46*, 900–906.

(67) Klein, N.; Zuccaro, C.; Dahne, U., Schultz, H.; Tellmann, N.; Kutzner, R.; Zaitsev, A.G.; Wordenweber, R. *J. Appl. Phys.* **1995**, *78*, 6683–6686.

(68) Tobar, M.E.; Krupka, J.; Ivanov, E.N.; Woode, R.A. *J. Appl. Phys.* **1998**, *83*, 1604–1609.

(69) Johnson, G.A.; Thompson, M.B.; Gewalt, S.L.; Hayes, C.E. *J. Magn. Reson.* **1986**, *68*, 129–137.

(70) Potter, K. *J. Cell. Biochem.* **2002**, *87*, 147–153.

(71) Wei, G.B.; Pettway, G.J.; McCauley, L.K.; Ma, P.X. *Biomaterials* **2004**, *25*, 345–352.

(72) Wong, H.M.; Wang, J.J.; Wang, C.H. *Ind. Eng. Chem. Res.* **2001**, *40*, 933–948.

(73) Peasley, M.A.; Shi, R.Y. *J. Neurolog. Sci.* **2003**, *216*, 23–32.

(74) Liu, J.Q.; Sham, J.S.K.; Shimoda, L.A.; Kuppusamy,

P.; Sylvester, J.T. *Am. J. Phys. Lung Cell. Mol. Physiol.* **2003**, *285*, L322–L333.

(75) Dobrucki, J.W. *J. Photochem. Photobiol. B* **2001**, *65*, 136–144.

(76) Zhong, W.; Urayama, P.; Mycek, M.A. *J. Phys. D*: *Appl. Phys.* **2003**, *36*, 1689–1695.

(77) Grucker, D. *Prog. Nucl. Magn. Reson. Spectrosc.* **2000**, *36*, 241–270.

(78) Swartz, H.M. *Bio. Soc. Trans.* **2002**, *30*, 248–252.

(79) Wisniewska, A.; Draus, J.; Subczynski, W.K. *Cell. Mol. Biol. Lett.* **2003**, *8*, 147–159.

(80) Subczynski, W.K.; Kusumi, A. *Biochim. Biophys. Acta* **2003**, *1610*, 231–243.

(81) Young, R.M.; Holowka, D.; Baird, B. *J. Biol. Chem.* **2003**, *278*, 20746–20752.

(82) Korlach, J.; Schwille, P.; Webb, W.W.; Feigenson, G.W. *Proc Natl. Acad. Sci. USA* **1999**, *96*, 8461–8466.

(83) Baumgart, T.; Hess, S.T.; Webb, W.W. *Nature* **2003**, *425*, 821–824.

(84) Ge, M.T.; Gidwani, A.; Brown, H.A.; Holowka, D.; Baird, B.; Freed, J.H. *Biophys. J.* **2003**, *85*, 1278–1288.

(85) Swamy, M.J.; Ciani, L.; Ge, M.T.; Smith, A.K.; Holowka, D.; Baird, B.; Freed, J.H. *Biophys. J.* **2006**, *90*, 4452–4465.

(86) Wu, M.; Holowka, D.; Craighead, H.G.; Baird, B. *Proc. Natl. Acad. Sci. USA* **2004**, *101*, 13798–13803.

(87) Schauer, D.A.; Desrosiers, M.F.; Kuppusamy, P.; Zweier, J.L. *Appl. Radiat. Isot.* **1996**, *47*, 1345–1350.

(88) Ishchenko, S.S.; Okulov, S.M.; Vorona, I.P. *Phys. Solid State* **1999**, *41*, 1100–1101.

(89) Romanyukha, A.A.; Mitch, M.G.; Lin, Z.C.; Nagy, V.; Coursey, B.M. *Radiat. Res.* **2002**, *157*, 341–349.

(90) Watt, G.A.; Newton, M.E.; Baker, J.M. *Diamond Relat. Mater.* **2001**, *10*, 1681–1683.

(91) Sano, T.; Umeda, F.; Hashimoto, T.; Nawata, H.; Utsumi, H. *Diabetologia* **1998**, *41*, 1355–1360.

(92) Matsumoto, K.; Utsumi, H. *Biophys. J.* **2000**, *79*, 3341–3349.

(93) Inoguchi, T.; Li, P.; Umeda, F., Yu, H.Y.; Kakimoto, M.; Imamura, M.; Aoki, T.; Etoh, T.; Hashimoto, T.; Naruse, M.; Sano, H.; Utsumi, H.; Nawata, H. *Diabetes* **2000**, *49*, 1939–1945.

(94) Kasazaki, K.; Yasukawa, K.; Sano, H.; Yamada, K.; Utsumi, H. *Appl. Magn. Reson.* **2003**, *23*, 585–595.

(95) Aboul-Enein, H.Y.; Kruk, I.; Lichszteld, K., Michalska, T.; Kladna, A.; Marczynski, S.; Olgen, S. *Luminescence* **2004**, *19*, 1–7.

(96) Yamato, M.; Egashira, T.; Utsumi, H. *Free Radical Biol. Med.* **2003**, *35*, 1619–1631.

(97) Yasukawa, K.; Kasazaki, K.; Hyodo, F.; Utsumi, H. *Free Radical Res.* **2004**, *38*, 147–155.

(98) Rizzi, C.; Samouilov, A.; Kutala, V.K.; Parinandi, N.L.; Zweier, J.L.; Kuppusamy, P. *Free Radical Biol. Med.* **2003**, *35*, 1608-1618.

(99) Pandian, R.P.; Parinandi, N.L.; Ilangovan, G.; Zweier, J.L.; Kuppusamy, P. *Free Radical Biol. Med.* **2003**, *35*, 1138–1148.

(100) Halpern, H.J.; Chandramouli, G.V.R.; Barth, E.D., Yu,

C.; Peric, M.; Grdina, D.J.; Teicher, B.A. *Cancer Res.* **1999**, *59*, 5836–5841.

(101) Gallez, B.; Mader, K.; Swartz, H.M. *Magn. Reson. Med.* **1996**, *36*, 694–697.

(102) Kuppusamy, P.; Li, H.Q.; Ilangovan, G., Cardounel, A.J.; Zweier, J.L.; Yamada, K.; Krishna, M.C.; Mitchell, J.B. *Cancer Res.* **2002**, *62*, 307–312.

(103) Jackson, S.K.; Thomas, M.P.; Smith, S.; Madhani, M.; Rogers, S.C.; James, P.E. *Faraday Discussions* **2004**, *126*, 103–117.

(104) Gallez, B.; Swartz, H.M. *NMR Biomed.* **2004**, *17*, 223–225.

(105) Tsien, R.Y.; Miyawaki, A. *Science* **1998**, *280*, 1954–1955.

(106) Cook, B.N.; Bertozzi, C.R. *Bioorg. Med. Chem.* **2002**, *10*, 829–840.

(107) Liang, Z.C.; Freed, J.H. *J. Phys. Chem. B* **1999**, *103*, 6384–6396.

(108) Freed, J.H. *ESR and molecular dynamics.* In *Biomedical ESR*, Eaton, S.S.; Eaton, G.R.; Berliner, L.J., Eds.; Kluwer: New York, 2004; pp 239–268.

(109) Klar, T.A.; Jakobs, S.; Dyba, M.; Egner, A.; Hell, S.W. *Proc. Natl. Acad. Sci. USA* **2000**, *97*, 8206–8210.

(110) Medalia, O.; Weber, I.; Frangakis, A.S.; Nicastro, D.; Gerisch, G.; Baumeister, W. *Science* **2002**, *298*, 1209–1213.

(111) Chen, S.G.; Branz, H.M.; Eaton, S.S.; Taylor, P.C.; Cormier, R.A.; Gregg, B.A. *J. Phys. Chem. B* **2004**, *108*, 17329–17336.

(112) Jedrecy, N.; von Bardeleben, H.J.; Zheng, Y.; Cantin, J.L. *Phys. Rev. B* **2004**, *69*, 041308(R).

(113) Nebel, C.E. *Semicond. Sci. Technol.* **2003**, *18*, S1–S11.

(114) Norris, D.J.; Yao, N.; Charnock, F.T.; Kennedy, T.A. *Nano Lett.* **2001**, *1*, 3–7.

(115) Naumova, O.V.; Smirnov, L.S.; Stas, V.F. *Semiconductors* **1997**, *31*, 847–851.

(116) Pietrass, T.; Gaede, H.C. *Adv. Mater.* **1995**, *7*, 826–832.

(117) Leung, I.J.H.; Michal, C.A. *Phys. Rev. B* **2004**, *70*, 035213.

(118) Bromberger, C.; Jansch, H.J.; Kuhlert, O.; Schillinger, R.; Fick, D. *Phys. Rev. B* **2004**, *69*, 245424.

(119) Cova, P.; Menozzi, R.; Portesine, M.; Bianconi, M.; Gombia, E.; Mosca, R. *Solid-State Electron.* **2005**, *49*, 183–191.

(120) Benchenane-Mehor, H.; Idrissi-Benzohra, M.; Benzohra, M.; Olivie, F. *Jpn J. Appl. Phys. Part 1* **2004**, *43*, 7572–7575.

(121) Grillenberger, J.; Grossner, U.; Svensson, B.G.; Albrecht, F.; Witthuhn, W.; Sielemann, R. *Phys. Rev. B* **2004**, *70*, 205209.

(122) Pintilie, I.; Pintilie, L.; Moll, M.; Fretwurst, E.; Lindstroem, G. *Appl. Phys. Lett.* **2001**, *78*, 550–552.

(123) Olafsson, H.O.; Sveinbjornsson, E.O.; Rudenko, T.E.; Tyagulski, I.P.; Osiyuk, I.N.; Lysenko, V.S. *Appl. Phys. Lett.* **2001**, *79*, 4034–4036.

(124) Beanland, R., *Ultramicroscopy* **2005**, *102*, 115–125.

(125) Nakashima, K.; Tateno, K. *J. Appl. Phys.* **(2004)**, *95*, 3443–3452.

438

(126) Umeda, T.; Toda, A.; Mochizuki, Y. *Europ. Phys. J. Appl. Phys.* **2004**, *27*, 13–19.

(127) Peto, G.; Molnar, G.; Kotai, E., Dezsi, I.; Karsteen, M.; Sodervall, U.; Willander, M.; Caymax, M.; Loo, R. *Appl. Phys. Lett.* **2002**, *81*, 37–39.

(128) Lee, S.; Hong, K. *J. Ceram. Proc. Res.* **2004**, *5*, 296–300.

(129) Zanola, P.; Bontempi, E.; Ricciardi, C.; Barucca, G.; Depero, L.E. *Mater. Sci. Eng. B* **2004**, *114–115*, 279–283.

(130) Wang, Y.; Du, X.L.; Mei, Z.X., Zeng, Z.Q.; Xu, Q.Y.; Xue, Q.K.; Zhang, Z. *J. Cryst. Growth* **2004**, *273*, 100–105.

(131) Burge, R.E.; Yuan, X.C.; Knauer, J.N.; Browne, M.T.; Charalambous, P. *Ultramicroscopy* **1997**, *69*, 259–278.

(132) Ueda, K. *Appl. Surf. Sci.* **2004**, 237, 636–640.

(133) Vearey-Roberts, A.R.; Steiner, H.J.; Evans, S., Cerillo, I.; Mendez, J.; Cabailh, G.; O'Brien, S.; Wells, J.W.; McGovern, I.T.; Evans, D.A. *Appl. Surf. Sci.* **2004**, *234*, 131–137.

(134) Ardenkjaer-Larsen, J.H.; Laursen, I.; Leunbach, I., Ehnholm, G.; Wistrand, L.G.; Petersson, J.S.; Golman, K. *J. Magn. Reson.* **1998**, *133*, 1–12.